JPP JOURNAL OF PROTEINS AND PROTEOMICS
6(2), 2015, pp. 173-182

Research Article

MOLECULAR DYNAMICS STUDIES ON MAMMALIAN APOMETALLOTHIONEINS

Roobee Garla, Mohinder Pal Bansal and Mohan Lal Garg

Department of Biophysics, Panjab University, Chandigarh, 160014, India

Abstract: Despite innumerable publications on metallothionein (MT), the literature on apo-MT is limited. Without the understanding of apo-MT, it is not possible to study the metallation process of MT which is the key process involved in various functions of MT like metal transfer and heavy metal detoxification. The functional role of apo-MT is related to its structure. Considering the difficulty of spectroscopic measurements of apo-MT, the molecular dynamic (MD) simulations of mammalian apo-MTs i.e. human MT1a and MT2, rabbit MT1a and MT2a and rat MT1 and MT2 (individual α and β domain as well as complete protein (i.e. connected βα)) in vacuum and water has been carried out using a linear strand of these proteins as starting geometry. The structural behavior of rat apo-MTs is different from that of human and rabbit apo-MTs. Both human apo-MTs and rabbit apo-MTs polypeptide backbone adopt an overall random coil structure except two small stretches of helix towards N-terminal after simulation in vacuum and water. Regardless of sequence homology of different mammalian MT isoforms, only the rat apo-MTs contain two stretches of helices towards the C-terminal. The extent of global folding of polypeptide backbone increases after 20 ns simulation in water that reduces its solvent exposed surface area.

***Keywords*:** Mammalian apo-MTs; molecular dynamics; structure; vacuum; water.

Introduction

Metallothioneins (MTs) are low molecular weight (6-7 kDa) metal binding proteins. MT superfamily is a collection of diverse proteins present in both eukaryotic and prokaryotic phyla with unclear phylogenetic relationships. Despite their unresolved evolutionary origins, MT sequences from different species share common characteristics like prevalence of cysteine residues (15-30%) arranged in characteristics CXC and CXXC motifs (Blindauer and Leszczyszyn, 2010). The three-dimensional structural investigations using ^{113}Cd- Nuclear Magnetic Resonance (NMR) and X-ray crystallography on mammalian MTs have established that MT contain two structurally independent domains, i.e. $M(II)_3S_9$ in the N-terminal, named the β domain and $M(II)_4S_{11}$ in the C-terminal, named the α domain (Arseniev *et al.*, 1988; Schultze *et al.*, 1988; Messerle *et al.*, 1990; Robbins *et al.*, 1991). All the cysteine residues participate in metal binding and each of the divalent metal ions is tetrahedrally coordinated to four cysteine thiolate sulfur atoms.

MT possess diverse metal binding preferences that help them in playing a crucial role in the homeostasis of essential metals like Zinc and Copper and in the protection against toxic non-essential metals such as Cd, Hg etc. (Tandon *et al.*, 2001; Klaassen *et al.*, 2009; Bell and Vallee, 2009). MT acts as an antioxidant against reactive oxygen species (ROS) and reactive nitrogen species (RNS). MT-III (also known as growth inhibitory factor) helps in providing protection against neurodegenerative diseases like

Corresponding Author: **Roobee Garla**
E-mail: rubygarla@yahoo.co.in

Received: January 14, 2015
Accepted: April 2, 2015
Published: April 5, 2015

Alzheimer's (AD), Parkinson's (PD) and prion (Kawashima *et al.*, 2000; Sogawa *et al.*, 2001; Hozumi *et al.*, 2004). The majority of research on MT to date has focussed on its fully metallated forms (Sutherland *et al.*, 2012). It is only in recent years; the physiological importance of partially metallated and apo forms of MT has been evolved.

Despite innumerable publications on MT, the literature on apo-MT is limited. The *in vitro* stability of apo-MTs is the main hurdle in their spectroscopic characterization and primary reason for the little attention paid to them. Only in last decade, fluorescence based methods have been developed that can quantitate apo-MT in *in vivo* conditions and has shown greater stability of apo-MTs in these conditions (Yang *et al.*, 2001). It has been found that the ratio of metallated MT to apo-MT plays a crucial role in the transfer of Zn from MT to other proteins such as mitochondrial aconitase, sorbitol dehydrogenase and transcription factor IIIa etc (Fischer and Davie, 1998; Krezel *et al.*, 2007). Inversely, the addition of apo-MT can restore the activity of enzymes in which Zn act as an inhibitor (Romero-Isart and Vasák, 2002). In a variety of tumors, a large fraction of MT exists as apo-MT and thus, opening additional perspectives on the functions of both, apo-MT and MT (Petering *et al.*, 2006). The *in vivo* stability of apo-MTs points towards their functional role in physiological conditions that is often related to the structure attained by the protein in these conditions.

The initial ^{1}H NMR studies on equine liver apo-MT1B done by Vasak *et al.*, (1980) showed that it possess a predominantly disordered structure. Recently, Summers *et al.*, had studied recombinant human apo MT2 (apo-rhMT2) using ESI-MS (Summers *et al.*, 2012). Their results showed that the mass spectra of Zn_7-rhMT2 and apo-rhMT2 at pH 7 exhibits the same charge state distribution, indicating that apo-rhMT2 can be folded like metallated protein, regardless of the lack of specific secondary or tertiary structure. Further structural studies are required on apo-MT.

Considering the difficulty of spectroscopic measurements of apo-MT, the molecular dynamics (MD) simulation is the most feasible approach to study the structure of apo-MTs. Studies are available in which MM3/MD were successfully used for the structural analysis of metallated-MTs (Fowle and Stillman, 1997; Berweger *et al.*, 2000; Rigby et al., 2006; Ngu *et al.*, 2008; Summers *et al.*, 2012). In addition to these studies, full QM structural analysis of both domains of human Metallothionein 2 (MT2) was also published, that not only reaffirmed the already known structural features of hMT2 from NMR and extended X-ray absorption fine structure (EXAFS) spectroscopies, but also provides a new physical insight with accurate accounts of bridging and terminal thiolate-metal bonds (Kepp, 2012). However, the data on the structural studies of apo-MTs in vacuum and water using MD calculations is scarce. Rigby and Stillman, (2004) carried the MD simulations of metal free recombinant human MT (rhMT) in vacuum using MM3/MD. Earlier investigations have reported that polypeptide backbone of rhMT adopts a random coil structure when started from linear strand. Another significant result was that human apo-MT showed retention of a significant degree of structural features upon demetallation. Moreover, the cysteinyl sulfurs, which were found buried within the domain of the protein when in the metallated state, were found to rotate to the exterior of the domain (Duncan and Stillman, 2006). Calculation on demetallated human apo-MT also show that the number of hydrogen bonds in both domains increases with sequential demetallation, which could help in structural stabilization (Duncan and Stillman, 2006; Rigby *et al.*, 2006).

Keeping in view the difficulty of spectroscopic measurements and limited literature available using MD simulation on apo-MT (mainly on human apo-MT2), the present work has been designed to study six mammalian apo-MT isoforms using the MD calculations. The apo forms of human MT1a and MT2, rabbit MT1a and MT2a and rat MT1 and MT2 (individual α and β domain as well as complete protein (i.e. connected $\beta\alpha$)) have been investigated. The simulation studies of apo-MTs in water closely reflect the cellular environment of apo-MTs and their structural evolution, while synthesized inside the cell. As the three dimensional structure of metallated MT is dependent on the metal binding

with sulfur of cysteine residues, the conformation attained by the apo-MTs helps to understand whether it is favorable to metallation or not. Comparison of structures obtained for different isoforms unravels whether any difference in structural behavior of apo-MTs occurs due to the variation in their amino acid sequences.

Materials and Methods

The sequence alignment of human MT1a and MT2, rabbit MT1a and MT2a and rat MT1 and MT2 were done using MULTALIGN programme (Corpet, 1988). All the MD calculations were performed using the GROMACS software package on a Red Hat Enterprise Linux 6 operating system on Fujitsu work station with dual Intel Hex core xenon X5660 2.8 GHz processor with 48 GB RAM (Spoel *et al.*, 2005). It is worth mentioning that the simulation results obtained by GROMOS force field are found to be in good agreement with the experiment for peptides and proteins (Stockner *et al.*, 2003; Todorova *et al.*, 2008; Blinov *et al.*, 2009). As there is no NMR/X-ray crystallographic structure available for apo-MTs, the apo forms of human MT1a and MT2, rabbit MT1a and MT2a and rat MT1 and MT2 (both individual α and β domain as well as complete protein i.e. connected βα) were synthesized using the sequence builder function in SPDBV in order to produce a linear strand of these proteins which were taken as the starting geometry for simulation studies (Guex and Peitsch, 1997). It resembles with the *de novo* synthesized apo-MT, prior to post-translational metallation. The stereochemical quality of the starting structures of these proteins was checked using ERRAT program before the MD simulation run length (Colovos and Yeates, 1993). The overall quality factor lies within the acceptable range.

Interaction parameters within the design sequence were taken from GROMOS-96 force field 43A1 best known for proteins (vanGunsteren *et al.*, 1996). Energy of the system was minimized by the Steepest Descent Method, with a gradient 50 kJ mol^{-1} followed by Conjugate Gradient method with a gradient of 20 kJ mol^{-1}. Next, the MD run was carried out in vacuum for 2 ns, with a time step of 2 ps using the Leap Frog Algorithm. The temperature was controlled through weak coupling to a bath of constant temperature using a coupling time; τ_p of 0.1 ps and a reference temperature; T_0 of 300 K (Berendsen *et al.*, 1984). The LINCS algorithm was used to restrict all bonds to their equilibrium lengths and the center of mass motion of the system was removed every step to maintain the effective simulation temperature at 300 K (Hess *et al.*, 1997). For the evaluation of short range electrostatic interactions and van der Waals interaction a cut off of 0.9 and 1.0 nm respectively was applied. Long range forces were updated every 10 fs during generation of the neighbor list. The Long Range Electrostatic Interactions were calculated using a Particle Mesh Ewald Summation. Initial velocities of all atoms were obtained from a Maxwellian distribution at the desired initial temperature. On the basis of the final conformation obtained for apo-MTs after 2 ns simulation in vacuum MD, a simple cubic periodic box was set up using the Simple Point Charge (SPC) Water Model (Berendsen *et al.*, 1981). For equilibration of solvent around the model proteins under study, their position was restrained for 20 ps. The simulation of apo-MT have been carried out initially for 2 ns and then, further for 20 ns in water. The pressure was controlled using weak coupling with a time constant of 0.5 ps and a reference pressure of 1 Bar. All figures were prepared using Pymol.

In addition to MD simulations, the Chou-Fasman, Garnier-Osguthorpe-Robson (GOR) and Qian and Sejnowski Algorithms were used to predict the secondary structure elements using the amino acid sequences of the above mentioned mammalian apo-MT isoforms (Prevelige and Fasman, 1989; Garnier *et al.*, 1978; Qian and Sejnowski, 1988).

Results and Discussion

Sequence divergence between the mammalian MTs

The sequence alignment and identity matrix of human MT-1a and MT-2, rabbit MT-1a and MT-2a and rat MT-1 and MT-2 is given in Figure 1 and Table 1, respectively. All the isoforms contain 61 amino acids except rabbit MT-2a which contain one insertion of ala at 8′ position. The sequence alignment revealed that out of 61 amino acids (62

Table 1
Sequence identity matrix of mammalian MT isoforms

	HumanMT 1-a	*HumanMT-2*	*RabbitMT-2a*	*RabbitMT-2b*	*RatMT-1*	*Rat MT-2*
Human MT-1a	100	88.5	86.9	82.3	80.3	83.6
Human MT-2	88.5	100	91.8	91.9	83.6	88.5
Rabbit MT-2a	86.9	91.8	100	87.1	85.2	85.2
Rabbit MT-2b	82.3	91.9	87.1	100	80.6	83.9
Rat MT-1	80.3	83.6	85.2	80.6	100	80.3
Rat MT-2	83.6	88.5	85.2	83.9	80.3	100

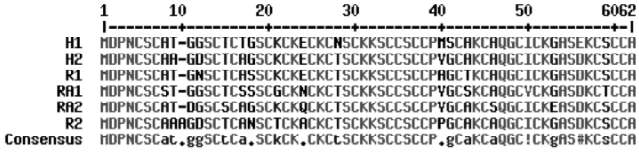

Figure 1: **Sequence alignments for the MT isoforms i.e. human apo-MT-1a and apo-MT-2 (H1 and H2), rabbit apo-MT-1a and apo-MT-2a (R1 and R2) and rat apo-MT-1 and apoMT-2 (RA1 and RA2) using MULTALIGN programme. (Red and uppercase - residue at that position is exactly same, Blue and lowercase- residues at that position are very similar, Red hash- residues are more or less similar, Black dot- dot- no common property)**

for rabbit MT-2a), 43 are conserved in all the isofoms, 9 are strongly similar, 4 are weakly similar and 5 are variable suggesting high homology between them. The sequence identity is above 80%, for the apo-MTs under the study.

MD simulations

MD simulations were performed individually on α and β domain as well as on complete protein (i.e. connected βα) in vacuum and water for 2 ns at 300 K. Analysis of the structures attained by α and β domains, and complete protein, in both the isoforms of all the species under study were done. We have found different structural patterns of polypeptide backbone of individual domains and complete protein mainly at the terminals of the α- and β- domains. This can be due to the extra flexibility at the additional C-terminal of β domain and N-terminal of α domain when they were considered individually. In case of metallated protein the structure pattern in individual domain is identical to the complete protein due to the constraints imposed on the polypeptide backbone to form the metal cluster which is absent in apo-MT. However, in nature, only the complete protein (i.e. connected βα) exists, therefore, the MD simulation results for the complete protein are biologically more relevant and discussed henceforth. In Figure 2, the root-mean-square deviation (RMSD) of the peptide backbone atoms, with respect to the initial structure are given as a function of time for all apo-MTs.

Apo-MT isoforms after 2 ns simulation in vacuum and water

The structures obtained at the end of simulations in vacuum as well as in water for human MT-1a and MT-2 are shown in Figure 3(a), (c) and Figure 3(b), (d) respectively. Human MT-1a polypeptide backbone is devoid of the secondary structure features except a small stretch of helix found at the N-terminal/β domain (residue number 2-8) after the simulation in vacuum. The molecular view of human MT-1a revealed that the surface area of the polypeptide backbone reduces after interacting with water molecules with no additional secondary structural features. In case of the human MT-2 (Figure 3(b)), again the overall structure of the protein in vacuum is mainly devoid of secondary structural features except for two small stretches of helices present in the β domain. After simulation in water, the helical structures were lost and instead turns appeared. Like human MT-1a, human MT-2 also became compact after interacting with water molecules.

Figure 4 shows the structures of rabbit MT-1a and MT-2a after 2 ns simulation in vacuum and water. In rabbit MT-1a (Figure 4(a)), the residues 4-14 are present in α-helical structure where as in rabbit MT-2a, in addition, another stretch of α-helical structure (residues 18-24) is present. A turn separates the two stretches. On interactions with water molecules after 2 ns simulation (Figure 4(b)), the rabbit MT-1a retains the α-helical structure at the N-terminal. The molecular view

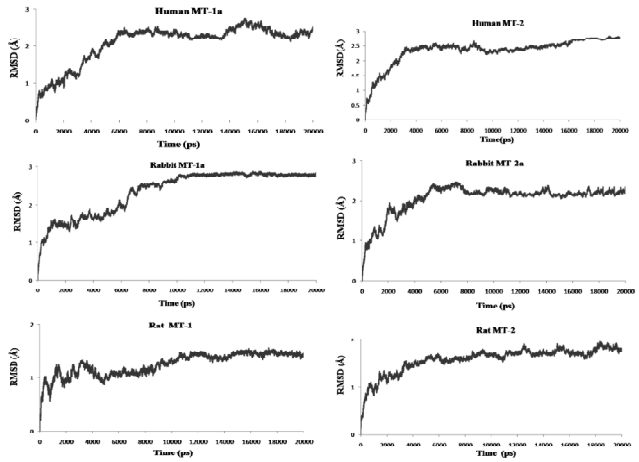

Figure 2: **Backbone RMSD for human apo-MT-1a and apo-MT-2, rabbit apo-MT-1a and apo-MT-2a and rat apo-MT-1 and apoMT-2 as function of the time.**

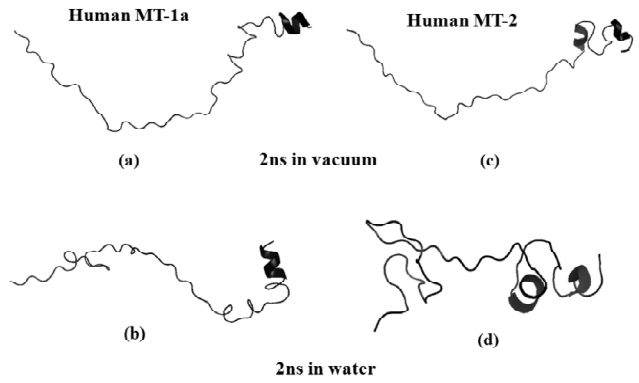

Figure 3: **Cartoon representation of human apo-MT1a and apo-MT2 after 2 ns simulation in vacuum (a) and (c) and 2 ns simulation in water (b) and (d), respectively at 300 K.**

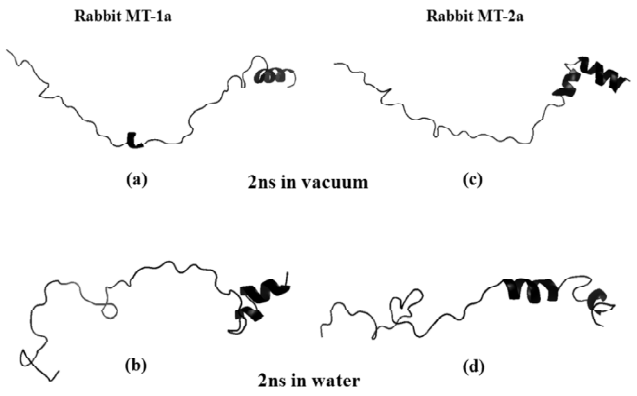

Figure 4: **Cartoon representation of rabbit apo-MT1a and apo-MT2a after 2 ns simulation in vacuum (a) and (c) and 2 ns simulation in water (b) and (d), respectively at 300 K.**

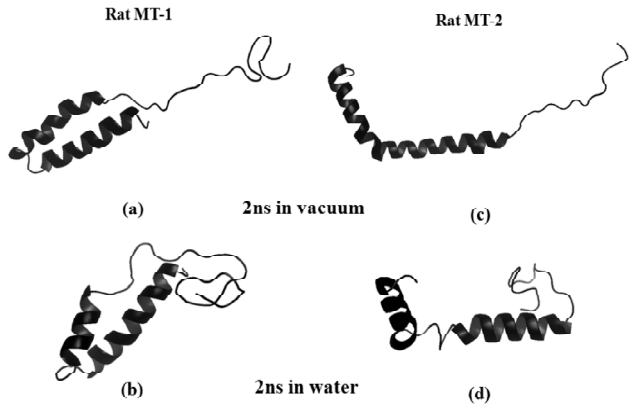

Figure 5: **Cartoon representation of rat apo-MT1 and apo-MT2 after 2 ns simulation in vacuum (a) and (c) and 2 ns simulation in water (b) and (d), respectively at 300 K.**

of rabbit MT-1a (Figure 4(a), (b)) shows that in vacuum, more or less its shape resembles to the shape of alphabet L whereas in water the shape changes to dumbbell type with the appearance of a turn at residues no 36-40. As a result of this, the overall polypeptide folding increased. For rabbit MT-2a, after interaction with water molecules (Figure 4(c),(d)), the number of amino acid residues (2-14) involved in α-helical stretch present at N terminal reduces to (5-9). Whereas the number of amino acids (14-18) forming the turns in vacuum increases to (10-21) in water followed by another helical stretch. In this case also, the extent of global folding of polypeptide backbone increases after interacting with water molecules.

The graphical views of rat MT-1 and MT-2 in vacuum and water after 2 ns simulation are shown in Figure 5. The views clearly depict the presence of two long stretches of α-helices present towards the C-terminal and in both the isoforms after simulation in the vacuum. The secondary structure elements were retained in both the isoforms after simulation in water towards the C-terminal end. However, towards the N-terminal, the backbone conformation of the polypetide appears to be linear and extended after 2 ns simulation in vacuum which becomes coiled after 2 ns simulation in water. As a result the folding of polypeptide increases which reduces the surface area of polypeptide exposed to water.

Apo-MT isoforms after 20 ns simulation in water

Figure 6 (a) and (b) shows the structure of human MT-1a and MT-2, respectively after 20 ns simulation in water. Both human MT-1a and MT-2 polypeptide backbones were devoid of the

secondary structure features except a small stretch of helix found at the N-terminal/β domain (residue number 2-8) after the 20 ns simulation in water. The structure obtained 20 ns simulation was significantly different from the structure obtained after 2 ns simulation in water for both isoforms (Figure 6(a), (b)). Although, for both the isoforms the overall structure of the polypeptide backbones were mainly devoid of secondary structural features.

The structures of rabbit MT-1a and MT-2a after 20 ns simulation in vacuum and water are shown in Figure 6 ((c), (d)). In rabbit MT-1a (Figure 6 (c)), an α-helical stretch was present at the C terminal (residues 53-57) and rest all the polypeptide backbone was devoid of any secondary structural feature. In rabbit MT-2a, two small stretches of α-helix (residues 5-10 and 13-18) were present (Figure 6 (d)). A turn was also present.

The graphical views of rat MT-1 and MT-2 in vacuum and water after 20 ns simulation are shown in Figure 6 ((e), (f)). Two stretches of α-helices towards the C-terminal involving residues 27-35 and 41-49 were observed in case of rat MT-1 after 20 ns simulation in water. On the other hand, rat MT-2 contained three small α-helical stretches involving residues 18-23, 28-37 and 51-56.

To explain the difference in secondary structure features in different apo-MTs, we had analyzed their amino acid sequences using different secondary structure prediction algorithms like Chou-Fasman, GOR and Neural Network (Prevelige and Fasman, 1989; Garnier *et al.*, 1978; Qian and Sejnowski, 1988). The site of Center for Informational Biology, Ochanomizu University (*http://cib.cf.ocha.ac.jp/bitool/MIX/*) was used for these predictions. According to these predictors, the polypeptide backbone of all apo-MTs should remain in random coil or devoid of any secondary structure.

Analysis of structures obtained as a function simulation time for apo-MT isoforms

In all the apo-MTs under study, the extent of global folding of polypeptide backbone increases as a function of simulation time in water. This fact is evident, when we analyze the structures of apo-MT at different time points. For human and rabbit apo-MTs, the extent of global folding of polypeptide backbone increases, but the variation in the numbers and positions of amino acids involved in conventional secondary structural elements was negligible (data not shown). The graphical views of rat apo-MT1 at different time points (i.e. 5 ns, 10 ns, 15 ns and 20 ns) reveals that the extent of global folding of polypeptide backbone increases and a significant difference was observed in the numbers and positions of amino acids involved in conventional secondary structural elements (Figure 7).

As the amino acid sequence homology in the different isoforms from different mammalian species is high (above 80%), it was expected that the conformational behaviour attained by different apo-MTs would be similar. But the results obtained after the MD simulations for both vacuum and water after 2 ns simulation suggest that the structural behaviour of rat apo-MTs is entirely different from that of human and rabbit apo-MTs. To explain the difference in secondary structure features in different apo-MTs, we analyzed their amino acid sequences using

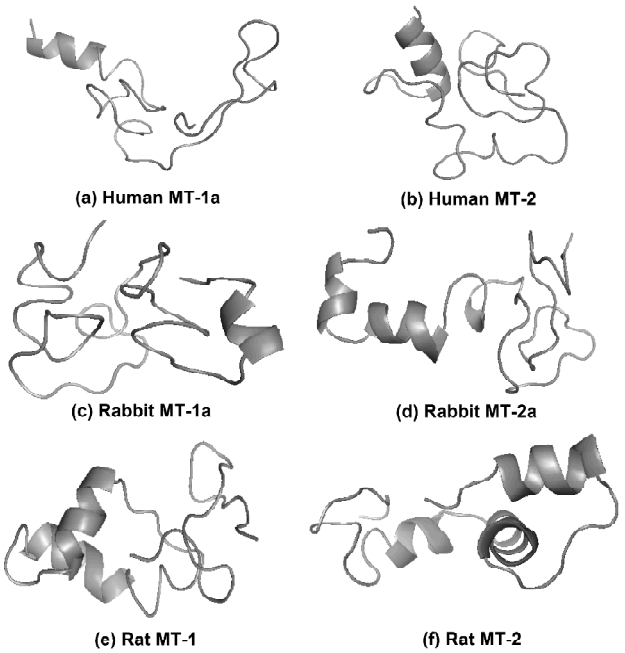

Figure 6: **Cartoon representation of (a) human apo-MT1a (b) human apo-MT2 (c) rabbit apo-MT1a (d) rabbit apo-MT2a (e) rat apo-MT1(f) rat apo-MT2 after 20 ns simulation in water at 300 K.**

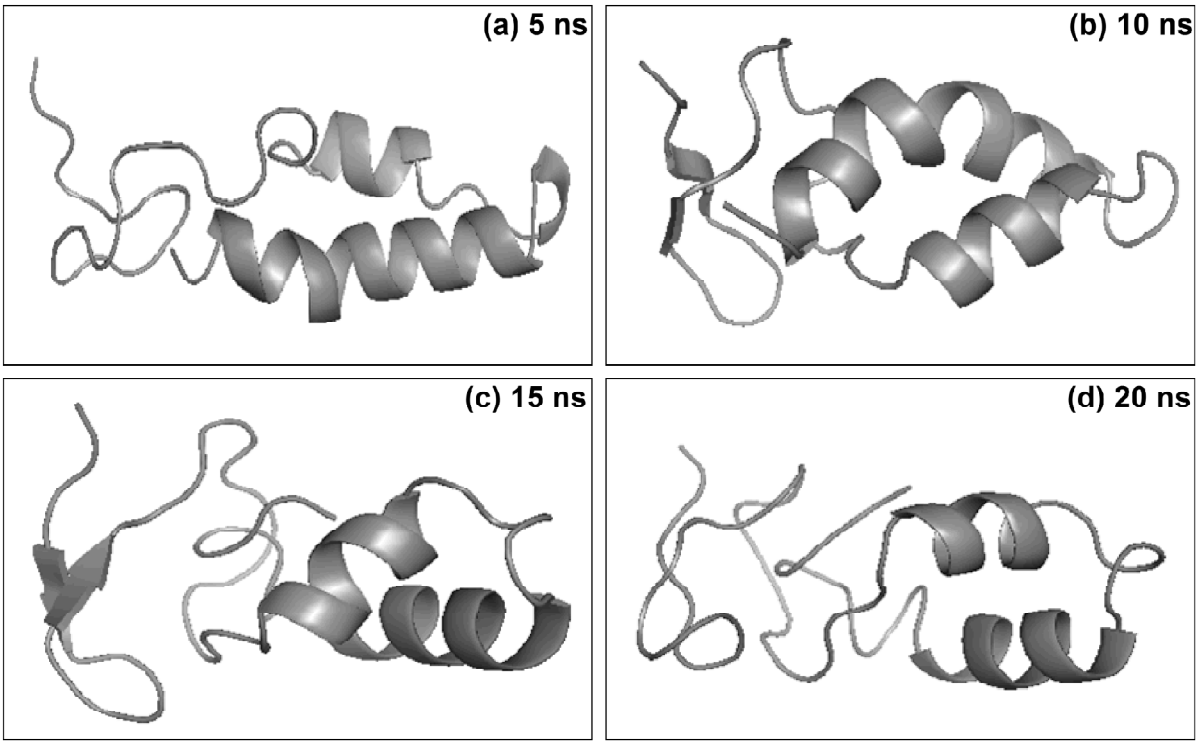

Figure 7: **Cartoon representation of rat apo-MT1 at different time points i.e. (a) 5 ns (b) 10 ns (c) 15 ns (d) 20 ns of simulation in water at 300 K.**

different secondary structure prediction algorithms like Chou-Fasman, GOR and Neural Network. These predictors were not able to explain the structural differences. However, when we compared 4-14 residues of rabbit apo-MTs (which formed helix) with rat apo-MTs (which did not form helix) we found that at residue 8 rabbit MT-1a and rabbit MT-2a contain alanine whose propensity for helix is very high (1.42) whereas rat MT-1 contains serine whose propensity for the helix is low (0.77). Moreover, at residue 11, rat MT-1contains glycine, which again has a very low propensity for helix (0.57) (Voet and Voet, 2004). These may be the reason for rat apo-MT1 not attaining the helical structure for amino acid residues 4-14. In rabbit MT-2a, at residues 38-40 a stretch of Pro-Pro-Gly, which are strong helix breakers, was found. This may be the cause for rabbit MT-2a not attaining the helical structures towards C-terminal present in the rat apo-MTs.

The observations that some structures are very different despite large similarities in sequence and the resemblance of the water structures with the vacuum structures for most of apo-MT isoforms (despite the fact they were started from them), made us to think that in case of apo-MTs 2 ns simulation in water perhaps was not sufficient for equilibration. Also, the computed results for rat apo-MT1 (producing alpha helix character) are inconsistent with the experimental finding of Bofil *et al.*, (2001), who reported that rat apo-MT1 is fully disordered without Zn(II) binding. In order to resolve this, the apo-MT isoforms were further simulated in water for 20 ns.

After 20 ns simulation in water, both human apo-MTs and rabbit apo-MTs attain random coil structure and were mainly devoid of any secondary structural elements except one/two small á-helical stretch(es) at the terminals. In solution, the terminals of the proteins are usually very flexible. Even for the NMR structures of human Cd_7MT2, rabbit Cd_7MT2a and rat Cd_7MT2, higher pairwise local root mean square deviation (r.m.s.d) values were observed for the terminal residues, among the 20 best fit structures as compared to the rest of the polypeptide backbone (Arseniev *et al.*, 1988; Schultze *et al.*, 1988; Messerle *et al.*, 1990). The extra flexibility of apo-MTs at the

terminals in water can be responsible for the appearance of helices in MD simulations. Therefore, we can say that both human apo-MTs and rabbit apo-MTs attain random coil structure after 20 ns simulation in water which is consistent with the experimental findings. Our results are similar to the findings of Rigby and Stillman, (2004) that carried MD simulations of recombinant human MT in vacuum using MM3/MD starting from linear strand geometry. These investigations also reported that the polypeptide backbone adopted a random coil conformation when started from linear strand. But, the small stretch of helix was not reported. This may be due to the different force field parameters used. Comparative data for the empirical force fields is not available for MTs. This type of data is available for insulin which is also low molecular weight protein like MT. The outcome of their results suggested that the all-atom force field CHARMM27 and the united-atom force field GROMOS 43A1 delivered the best representation of the experimentally observed behaviour of insulin (Todorova *et al.,* 2008).

For the rat MT-1 and MT-2, the helical stretches were present even after 20 ns simulation in water. Although, the number of amino acids involved in these structures were reduced significantly. These findings are inconsistent with the results of Bofil *et al.*, (2001). They did not find any peak corresponding to helices in the CD spectra of rat apo-MT1 at pH 3. Recent studies of Summers *et al.*, (2012) had shown that the structure of apo-MTs is quite different at pH 3 and 7. In MD calculations, the pH factor was not included. This might be the reason for the structural difference. As the number of amino acids involved in helical structures in rat apo-MTs are significantly reduced after 20 ns simulation as compared to the structure after 2 ns. It might be possible that even 20 ns simulation in water is not enough for the equilibration of rat apo-MTs.

The structural divergence of apo-MTs in the presence of sequence similarity can be due to the similar phenomenon observed in intrinsically disordered proteins. Borcherds *et al.*, (2013) observed that the MDM2 binding sites of the p53 transactivation domain (p53TAD) show weak correlation between the secondary structure and sequence identity matrix. For example, the sequence identity between the murine double minute 2 (MDM2) binding sites of the p53TAD of human and dog is 85% hinting towards their structural similarity. However, the NMR spectrum obtained for alpha carbon chemical shifts show the presence of helical structure for human MDM2 binding site of p53TAD and no such structural feature for the dog. The conformations attained by intrinsically disordered proteins are sensitive to change in solvents. Amyloid Aβ42 proteins (one of the intrinsically disordered proteins) adopt a disordered coil-turn rich structure in aqueous solution and adopt an ordered helical conformation in apolar solvents (Crescenzi *et al.*, 2002; Tomaselli *et al.*, 2006). In our study also, the structures obtained for apo-MTs in vacuum are different from structures obtained after 20 ns simulation in water.

The structures obtained also suggest that the overall peptide fold is different for apo-MTs from different species. Such behaviour was not present in the metallated-MTs of same species (Arseniev *et al.*, 1988; Schultze *et al.*, 1988; Messerle *et al.*, 1990). This may be due to the formation of metallated core where only the cysteine residues are involved for metal binding and their number and position are highly conserved in all mammalian MTs which impose constraints on the folding of rest of the amino acids. In case of apo-MTs, no such constraints are imposed which leads to their extra flexibility and structural divergence.

In conclusion, MD simulations of apo-MTs in vacuum and water revealed that their structural behavior is dissimilar for different species which cannot be explained on the basis of their low (less than 20%) sequence divergence. The extent of global folding of polypeptide backbones increases as function of simulation time in water. Further studies are required in order to check the robustness of MD simulations.

Acknowledgments

This work is funded by University Grant Commission (UGC), New Delhi, India vide grant no. F. No. 37-317/2009 (SR). Department of Science and Technology, New Delhi, India is gratefully acknowledged for providing workstation facility at Department of Biophysics, Panjab University, Chandigarh under the DST-FIST grant. Roobee Garla is

thankful to UGC for providing financial assistance in the form of Junior/Senior Research Fellowship.

References

Arseniev, A., Schultze, P., Wörgötter, E., Braun, W., Wagner, G., Vasák, M., Kägi, J.H., and Wüthrich, K. (1988). Three-dimensional structure of rabbit liver [Cd_7] metallothionein-2a in aqueous solution determined by nuclear magnetic resonance. J Mol Biol 201, 637-657.

Bell, S.G., and Vallee, B. L. (2009). The metallothionein/thionein system: an oxidoreductive metalbolic zinc link. Chem Bio Chem 10, 55–62.

Berendsen, H.J.C., Postma, J.P.M., Dinola, A., and Haak, J.R. (1984). Molecular dynamics with coupling to an external bath. J Chem Phy 81, 3684-3690.

Berendsen, H.J.C., Postma, J.P.M., van Gunsteren, W.F., and Hermans, J. (1981). Interaction models for water in relation to protein hydration. In: Intermolecular Forces. (pp 331-342). Dordrecht: D Reidel Publishing Company.

Berweger, C.D., Thiel, W., and van Gunsteren, W.F. (2000). Molecular-dynamics simulation of the β domain of metallothionein with a semi-empirical treatment of the metal core. Proteins 41, 299–315.

Blindauer, C.A., and Leszczyszyn, O.I. (2009). Metallothioneins: unparalleled diversity in structures and functions for metal ion homeostasis and more. Nat Prod Rep 27, 720–741.

Blinov, N., Berjanskii, M., Wishart, D.S., and Stepanova, M. (2009). Structural Domains and Main-Chain Flexibility in Prion Proteins. Biochemistry 48, 1488–1497.

Bofill, R., Capdevila, M., Cols, N., Atrian, S., and Gonzàlez-Duarte, P. (2001). Zinc (II) is required for the in vivo and in vitro folding of mouse copper metallothionein in two domains. J Biol Inorg Chem 6, 405–417.

Borcherds, W., Kashtanov, S., Wu, H., and Daughdrill, G.W. (2013). Structural divergence is more extensive than sequence divergence for a family of intrinsically disordered proteins. Proteins 81, 1686–1698.

Colovos, C., and Yeates, T. O. (1993). Verification of protein structures: patterns of nonbonded atomic interactions. Protein Sci. 2, 1511-1519.

Corpet, F. (1988). Multiple sequence alignment with hierarchical clustering. Nucl. Acids Res. 16, 10881-10890.

Crescenzi, O., Tomaselli, S., Guerrini, R., Salvadori, S., D'Ursi, A.M., Temussi, P.A., and Picone, D. (2002). Solution structure of the Alzheimer amyloid β-peptide (1–42) in an apolar microenvironment; Similarity with a virus fusion domain. Eur J Biochem 269, 5642–5648.

Duncan, K.E.R., and Stillman, M.J. (2006). Metal-dependent protein folding: Metallation of metallothionein. J Inorg Biochem 100, 2101–2107.

Fischer, E.H., and Davie, E.W. (1998). Recent excitement regarding metallothionein. Proc Natl Acad Sci 95, 3333–3334.

Fowle, D.A., and Stillman, M.J. (1997). Comparison of the structures of the metal-thiolate: Binding site in Zn(II)-, Cd(II)-, and Hg(II)-Metallothioneins using molecular modeling techniques. J Biomol Struct Dyn 14, 393–406.

Garnier, J., Osguthorpe, D.J., and Robson, B. (1978). Analysis of the accuracy and implications of simple methods for predicting the secondary structure of globular proteins. J Mol Biol 120, 97-120

Guex, N., and Peitsch, M.C. (1997). SWISS-MODEL and the Swiss-PdbViewer: An environment for comparative protein modeling. Electrophoresis 18, 2714–2723.

Hess, B., Bekker, H., Berendsen, H.J.C., and Fraaije, J.G.E.M. (1997). LINCS: A linear constraint solver for molecular simulations. J Comp Chem 18, 1463-1472.

Hozumi, I., Asanuma, M., Yamada, M., and Uchida, Y. (2004). Metallothioneins and neurodegenerative diseases. J Health Sci 50, 323–331.

Kawashima, T., Doh-ura, K., Torisu, M., Uchida, Y., Furuta, A., and Iwaki, T. (2000). Differential Expression of Metallothioneins in Human Prion Diseases. Dement Geriatr Cogn Disord 11, 251–262.

Kepp, K.P. Full quantum-mechanical structure of the human protein Metallothionein-2. (2012). J Inorg Biochem 107, 15–24.

Klaassen, C.D., Liu, J., and Diwan, B.A. (2009). Metallothionein protection of cadmium toxicity. Toxicol Appl Pharmacol 238, 215–220.

Krezel, A., Hao, Q., and Maret, W. (2007). The zinc/thiolate redox biochemistry of metallothionein and the control of zinc ion fluctuations in cell signaling. Arch Biochem Biophys 463, 188–200.

Maret, W., Jacob, C., Vallee, B.L., and Fischer, E.H. (1999). Inhibitory sites in enzymes: zinc removal and reactivation by thionein. Proc Natl Acad Sci 96, 1936-1940.

Margoshes, M., and Vallee, B.L. (1957). A cadmium protein from equine imaging hyper-intensity in Alzheimer's disease: correlation with kidney cortex. J Am Chem Soc 79, 4813-4814.

Messerle, B.A., Schäffer, A., Vasák, M., Kägi, J.H., and Wüthrich, K. (1990). Three-dimensional structure of human [$^{113}Cd_7$] metallothionein-2 in solution determined by nuclear magnetic resonance spectroscopy. J Mol Biol 214, 765-779.

Ngu, T.T., Easton, A., and Stillman, M.J. (2008). Kinetic analysis of arsenic-metalation of human metallothionein: significance of the two-domain structure. J Am Chem Soc 130, 17016–17028.

Petering, D.H., Zhu, J., Krezoski, S., Meeusen, J., Kiekenbush, C., Krull, S., Specher, T., and Dughish, M. (2006). Apo-metallothionein emerging as a major player in the cellular activities of metallothionein. Expl Biol Med 231, 1528–1534.

Prevelige, P., and Fasman, G.D. (1989). Chou-Fasman Prediction of the Secondary Structure of Proteins: The Chou-Fasman-Prevelige Algorithm. In: Fasman GD

editor. Prediction of Protein Structure and the Principles of Protein Conformation. (pp 391-416). Plenum, New York.

Qian, N., and Sejnowski, T.J. (1988). Predicting the secondary structure of globular proteins using neural network models. J Mol Biol 202, 865-884.

Rigby, K.E., and Stillman, M.J. (2004). Structural studies of metal-free metallothionein. Biochem Biophys Res Comm 325, 1271–1278.

Rigby, K.E., Chan, J., Mackie, J., and Stillman, M.J. (2006). Molecular dynamics study on the folding and metallation of the individual domains of metallothionein. Proteins 62, 159–172.

Robbins, A.H., McRee, D.E., Williamson, M., Collett, S.A., Xuong, N.H., Furey, W.F., Wang, B.C., and Stout, C.D. (1991). Refined Crystal Structure of Cd, Zn metallothionein at 2.0 Å resolution. J Mol Biol 221, 1269-1293.

Romero-Isart, N., and Vasák, M. (2002). Advances in the structure and chemistry of metallothioneins. J Inorg Biochem 88, 388-396.

Schultze, P., Wörgötter, E., Braun, W., Wagner, G., Vasák, M., Kägi, J.H., and Wüthrich, K. (1990). Conformation of [Cd_7]-metallothionein-2 from rat liver in aqueous solution determined by nuclear magnetic resonance spectroscopy. J Mol Biol 203, 251-268.

Sogawa, C.A., Asanuma, M., Sogawa, N., Miyazaki, I., Nakanishi, T., Furuta, H., and Ogawa, N. (2001). Localization, regulation, and function of metallothionein-III/growth inhibitory factor in the brain. Acta Medica Okayama 55, 1–9.

Spoel, D.V., Lindahl, E., Hess, B., Buuren, A.R.V., Apol, E., Meulenhoff, P.J., Tieleman, D.P., Sijbers, A.L.T.M., Feenstra, K.A., Drunen, R.V., and Berendsen, H.J.C. (2005). GROMACS User Manual version 3.3.

Stockner, T., Sterk, H., Kaptein, R., and Bonvin, A.M.J.J. (2003). Molecular Dynamics Studies of a Molecular Switch in the Glucocorticoid Receptor. J Mol Biol 328, 325–334.

Summers, K.L., Mahrok, A.K., Dryden, M.D.M., and Stillman, M.J. (2012). Structural properties of metal-free apometallothioneins. Biochem Biophys Res Comm 425, 485–492.

Sutherland, D.E.K., Summers, K.L., and Stillman, M.J. (2012). Noncooperative metalation of metallothionein 1a and its isolated domains with zinc. Biochemistry 51, 6690–6700.

Tandon, S.K., Singh, S., Prasad, S., and Mathur, N. (2001). Hepatic and renal metallothionein induction by an oral equimolar dose of zinc, cadmium or mercury in mice. Food Chem Toxicol 39, 571–577.

Thompson, J.D., Higgins, D.G., and Gibson, T.J. (1994). CLUSTAL W: improving the sensitivity of progressive multiple sequence alignment through sequence weighting, positions-specific gap penalties and weight matrix choice. Nuc Acid Res 22, 4673-4680.

Todorova, N., Legge, F.S., Treutlein, H., and Yarovsky, I. (2008). Systematic Comparison of Empirical Forcefields for Molecular Dynamic Simulation of Insulin. J Phys Chem B 112, 11137–11146.

Tomaselli, S., Esposito, V., Vangone, P., van Nuland, N.A., Bonvin, A.M., Guerrini, R., Tancredi, T., Temussi, P.A., and Picone, D. (2006). The alpha-to-beta conformational transition of Alzheimer's Abeta-(1-42) peptide in aqueous media is reversible: a step by step conformational analysis suggests the location of beta conformation seeding. ChemBioChem 7, 257–267.

vanGunsteren, W.F., Billeter, S.R., Eising, A.A., Hünenberger, P.H., Krüger, P., Mark, A.E., Scott, W. R.P., and Tironi, I.G. (1996). Biomolecular Simulation: The GROMOS96 manual and and User Guide. ETH Zurich and BIOMOS b.v; Zurich: Gronigen.

Vasak, M., Galdes, A., Hill, H.A.O., Kagi, J.H.R., Bremner, I., and Young, B.W. (1980). Investigation of the Structure of Metallothioneins by Proton Nuclear Magnetic Resonance Spectroscopy. Biochemistry 19, 416–425.

Voet, D., and Voet, J.G. (2004). Biochemistry. John Wiley and Sons, New York, pp 300. 4th edition.

Yang, Y., Maret, W., and Vallee, B.L. (2001). Differential fluorescence labeling of cysteinyl clusters uncovers high tissue levels of thionein. Proc Natl Acad Sci 98, 5556-5559.